

IMECE2004-61695

PERFORMANCE AND DEVELOPMENT OF A MINIATURE ROTARY SHAFT PUMP (RSP)

Daniel B. Blanchard

Phillip M. Ligrani

Bruce K. Gale

Convective Heat Transfer Laboratory, Mechanical Engineering Department, University of Utah
50 S. Central Campus Drive Rm 2110, Salt Lake City, UT 84112
Tel.: 801-581-4240, Fax: 801-585-9826

ABSTRACT

The development and performance of a novel miniature pump called the rotary shaft pump (RSP) is described. The impeller is made by boring a hole in one end of a shaft, and cutting slots in the side of the shaft at the bottom of the bored hole, such that the metal between the slots defines the impeller blades. Several impeller designs are tested over a range of operating conditions. Pump performance characteristics, including pressure rise, efficiency, slip factor, and flow rate are presented for several different pump configurations, with maximum flow rate and pressure rise of 64.9ml/min, and 2.1kPa, respectively, when the working fluid is water. Potential applications include transport of biomedical fluids, drug delivery, total analysis systems, and electronics cooling.

INTRODUCTION

The area of microfluidics is developing with many new sensors, separation devices, drug delivery systems, and other small-scale and micro-scale fluidic devices. For many of these devices there is a need to circulate or move fluid through macro-scale and micro-scale channels. A variety of micropumps are available to meet this need, generally to fulfill specific applications [1]. These include membrane pumps [2], electrohydrodynamic (EHD) pumps [3], electrokinetic (EK) pumps [4], rotary pumps [5-8], peristaltic pumps [9], bubble based pumps [10], and several other types of pumps [1]. Other small-scale pumps have been developed for uses as blood pumps in ventricular assist devices [11-13]. Non-mechanical pumps like the electrohydrodynamic and electrokinetic pumps do not have moving parts, which increases reliability. However, such devices are generally limited by low flow rate and pressure rise capabilities, the applications of the pump, the working fluids that can be pumped, and high supply voltage requirements [1]. Mechanical pumps like rotary pumps, peristaltic pumps, and membrane pumps have a wide variety of possible working fluids and applications. However, such mechanical micro-pumps (like rotary micropumps) are believed to be feasible only when they are greater than a certain size [1].

One motivation of the present effort is to demonstrate the operation and feasibility of a millimeter-scale pump which imposes fluid motion and pressure rise by means of viscous and inertial forces. The behavior and performance of macro-scale centrifugal pumps are well established and well known. However, the dynamics, performance, and efficiency of centrifugal pumps change as the size of the pump is altered. For example, secondary flows, and the losses associated with them, become more important as macro-scale impeller passage size decreases. As size decreases further, surface (viscous) forces become more significant [14], and can dominate the performance of the pump. However, this does not appear to prevent the operation of the centrifugal micro-pumps and mini-pumps developed by Ahn [8] and Hainan [5]. The micropump by Ahn [8] is a radial inflow – radial outflow design, and is powered by an integrated magnetic micromotor with a 12 pole, 500 μ m diameter stator that also acts as the impeller. The advantage of this pump is the integrated magnetic motor, which also serves as a completely sealed pumping chamber with no leaks. This pump reaches a maximum flow rate of 24 μ l/min, with a maximum theoretical pressure rise of 100 Pa. The mini-pump by Hainan [5] is a centrifugal pump with an axial inflow and a radial outflow configuration. This pump is created using precision machining techniques, and measures 6 mm by 12 mm in size. This axial inflow, radial outflow pump produces a maximum flow rate of 100 ml/min, with a maximum pressure rise of 10 kPa. One disadvantage of this micropump is the potential leakage at the shaft/pump housing interface, which creates losses and reductions in performance. Some test data is provided by Ahn and Hainan, but extensive performance data for these pumps are not provided, nor are any details given regarding efforts to optimize the pump and impeller designs.

The present paper presents a novel rotary pump that has a 2.38 mm diameter impeller and high efficiency at low flow rates. The design modifications [15], relative to other small-scale centrifugal devices, include the impeller integrated into the body of the shaft, instead of on the top of the shaft. This design is unique and novel because of its simplicity, which

allows it to be easily manufactured at low cost, and because all problems of tip blade clearance and flow leakage around the blade tips are not present. Pump performance is characterized since the pressure rise, flow rate, and the efficiency/slip factor product are given for a wide range of impeller speeds and impeller configurations. Tested impeller designs include radial 2-blade, radial 4-blade, radial 6-blade, backward-curved 4-blade, and forward curved 4-blade arrangements. The fluid flow for each impeller design is throttled using outlet tubing diameters of 0.254 mm, 0.508 mm, and 1.397 mm of the same length. The present pump, or a variation of it, is useful for a variety of micro-biological and bio-medical analysis systems, electronics cooling, and drug delivery devices. For example, a larger-scale version of this pump has potential use as a blood pump for a ventricular assist device.

NOMENCLATURE

D	inner diameter of tubing
D_2	outer diameter of impeller
g	gravitational constant
H	actual pumping head
h	height of blades
H_{id}	ideal head
ΔP	pressure rise across pump impeller
Q	volumetric flow rate
U_2	outer blade tip velocity

Greek Symbols

β	blade tip angle
β_1	inner blade tip angle
β_2	outer blade tip angle
η	hydraulic efficiency
ρ	density
σ	slip factor
$\eta\sigma$	product of hydraulic efficiency and slip factor

PUMP PERFORMANCE

Parameters which characterize pump performance include head pressure rise, volumetric flow rate, overall slip factor magnitude, and hydraulic efficiency. The Euler equation relates pumping head to impeller geometry, speed of the impeller, and the flow rate of the fluid [16], and is given by

$$H_{id} = \frac{U_2^2}{g} - \frac{U_2 \cot(\beta_2) Q}{\pi D_2 h g} \quad (1)$$

$$H = H_{id} \eta \sigma \approx \frac{\Delta P}{\rho g} \quad (2)$$

Many of these parameters can be related to the geometry of a radial-flow impeller which is shown in Figure 1. With radial impeller designs, $\beta_2 = 90$ degrees, and the second term in Eq. (1) is zero. The ideal pumping head, as the flow rate increases, for a constant rotational speed, is then the horizontal line shown in Figure 2. With forward curved impeller designs, $\beta_2 > 90$ degrees, and for a constant speed, the ideal pumping head increases as the flow rate increases. Backward curved impeller designs have $\beta_2 < 90$ degrees, and the ideal pumping head decreases as flow rate increases for constant impeller rotational speed.

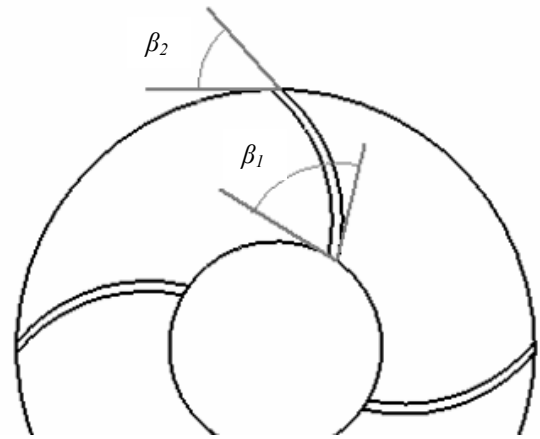


Figure 1. Impeller blade configuration and angles.

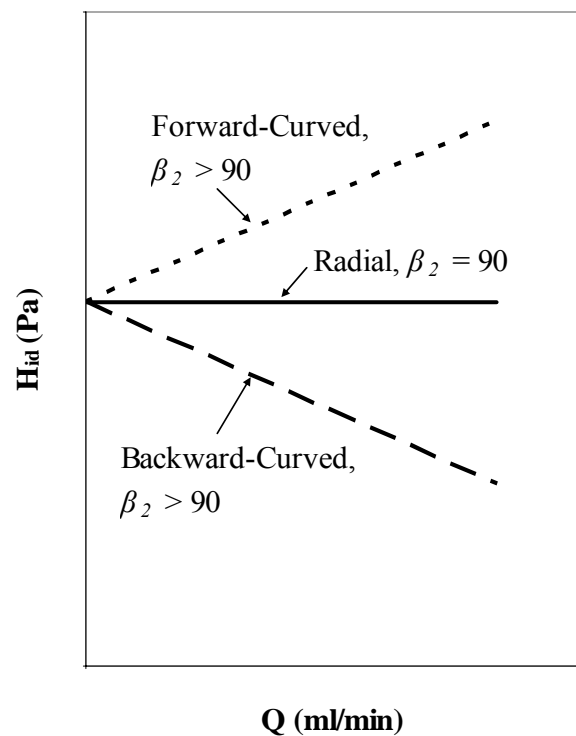


Figure 2. Idealized trends of pressure rise and flow rate for different impeller designs

Hydraulic efficiency is the ratio of energy added to the fluid between the outlet and inlet of the pump and the energy contained in the rotating impeller. The slip factor quantifies a decrease in ideal pumping head which occurs as the flow “slips” or deviates from the contours of the impeller blades. The slip factor is defined as the ratio of the tangential components of the absolute fluid velocity at the outer blade tip for flow with and without slip [17]. The product of hydraulic efficiency and slip factor is used to relate experimentally determined actual head of the rotary shaft pump to the theoretical head, given by Eq. (1). Equation (2) shows the relationship between the experimental and ideal pressure head. The pumping head corresponds to the increase in total pressure

of the fluid as it passes through the impeller. Static pressure measurements are made at pressure ports 1 and 2 shown in Fig. 4. The dynamic pressure at ports 1 and 2 are estimated by dividing the volumetric flow rate by the cross-sectional area of the passage at the pressure ports. The change in dynamic pressure is insignificant relative to the change in static pressure between pressure ports 1 and 2 and the pressure change due to the difference in vertical position of pressure ports 1 and 2 is negligible. Thus the rise in static pressure between pressure ports 1 and 2 represents the rise in total pressure across the pump impeller (pumping head). The product of hydraulic efficiency and slip factor is then determined using Eq. (2). The product of hydraulic efficiency and slip factor is used to characterize the performance of the different impeller designs and pump configurations.

PUMP CONFIGURATION AND GEOMETRY

One important dimension of many centrifugal pumps is the gap distance between the top of the blades, and the pump housing. As the gap increases, there is more leakage across blades, and the overall hydraulic efficiency of the pump decreases. If the gap is too small or zero, the blades can be damaged by contacting the pump housing. On a macro-scale this “gap problem” is generally insignificant, but on a micro-scale, or a millimeter-scale, the gap between the top of the blades and the pump housing can be about the same as the height of the impeller blades.

The design of the rotary shaft pump (RSP) eliminates this “gap problem.” The RSP impeller is constructed by boring a hole in the end of a shaft, and then cutting slots in the side of the shaft at the bottom of the bored hole, as shown in Figure 3 which presents a cutaway view of the RSP impeller. Thus, the metal between the slots acts as the blades of the impeller, and the slots form passages between the bored interior and outer shaft surface. The gap at the top of the blades is zero, because the top of the blades also connect to the shaft. The hollow interior of the RSP transfers momentum to the passing fluid through viscous forces. This “pre-swirl” can be significant on a millimeter-scale or micrometer-scale, when the ratio of the hollow interior length to diameter is large, and the circumferential wall velocity is greater than the average axial fluid velocity. The “pre-swirl” aids in the overall fluid pumping by reducing the sudden acceleration of the fluid at the inner blade tip, which reduces the flow separation at the leading edge of the impeller blade due to the incidence.

The rotating shaft is mounted using bearings located above and below the exit plenum, which are mounted in the pump housing. The volute and an outlet channel are then located in the region between the upper and lower bearings and pump housing, as seen in Figure 4. The water reservoir is connected to the pump housing by a plastic tube with an inner diameter of 4.5 mm and a length of 381 mm. This plastic tube is press fit into the inlet channel as shown in Fig. 4. There is a continuous channel, from the inlet tubing, through the pump housing and top of the upper bearing to the inlet of the RSP. Inside the channel through the upper bearing, the fluid flow transitions from a non-rotating bearing wall to the inside of a rotating shaft. The bearing forms a seal for the spinning shaft of the RSP, which reduces the leakage from the impeller outlet to the shaft inlet of the RSP. The side walls of the volute and part of the outlet channel are formed by a piece of machined brass

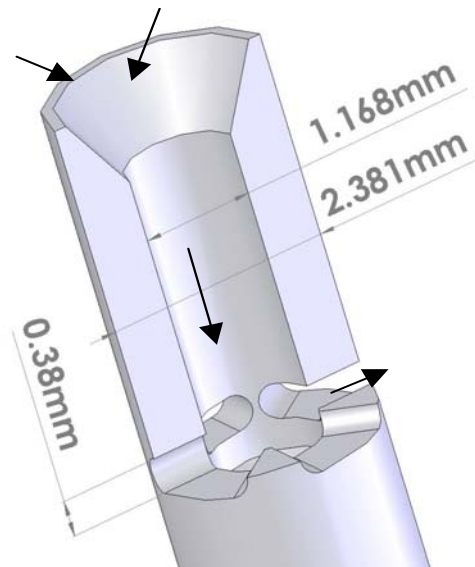


Figure 3. Cutaway view of the rotary shaft pump (RSP) impeller. Shown in the radial 4-blade impeller. Arrows indicate flow direction.

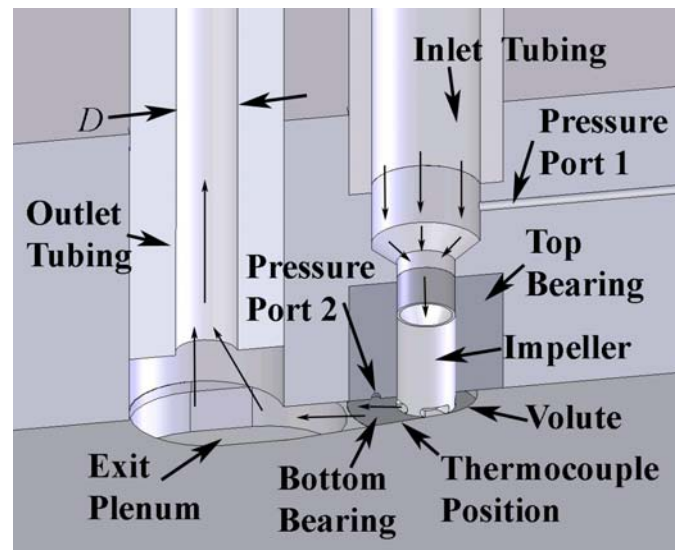


Figure 4. Cutaway view of the rotary shaft pump (RSP) assembly.

shim stock that is 416 μm tall. This volute and outlet channel is aligned with the slot ports of the shaft. With this construction, when the shaft spins, centrifugal forces from the spinning impeller shaft forces fluid flow through the shaft inlet, through the interior of the shaft, through the slots, out through the slot ports, into the volute, and then into and through the outlet channel, as shown by the arrows in Fig. 4. The volute design employed for the present investigation, to minimize the effects of surface forces, is called the open volute design. The open volute design is characterized by a large “open” channel from the impeller to the exit plenum, as shown in Figure 5.

One of the purposes of a volute is to efficiently direct fluid toward the outlet channel. The volute designs employed in macroscale pumps, where fluid motion is induced by inertial forces, are different from the design employed here. This design difference is because flow from the impeller exit and

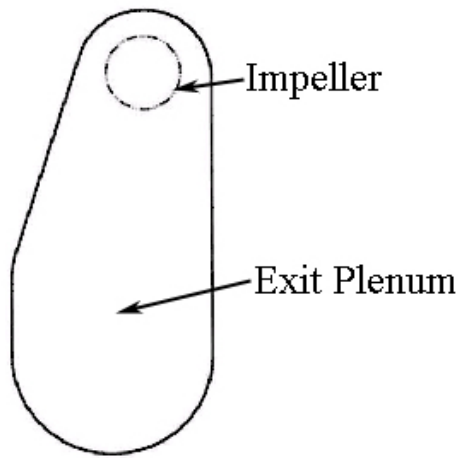


Figure 5. Open volute configuration.

within the volute is significantly influenced by both inertial forces and surface forces. The present open volute design increases the width and maximizes the hydraulic diameter thereby decreasing the average fluid velocity and velocity gradients, which also reduces viscous losses.

PUMP COMPONENT FABRICATION

There are five main fabricated components of the rotary shaft pump assembly: (i) the impeller, (ii) top housing, (iii) bottom housing, (iv) bearings, and (v) volute.

Fabrication of the impeller is realized using precision machining techniques. A lathe is used to obtain the desired outside diameter of the shaft, and to bore the hole in the end of the shaft. The cone shape at the inlet of the shaft is made using a center drill. Slots are then cut into the side of the shaft using a milling machine and an indexing tool. The impeller is made from 304 stainless steel. Five impeller designs are constructed for testing: radial 2-blade, radial 4-blade, radial 6-blade, backward curved 4-blade, and forward curved 4-blade. The blades are evenly spaced around the circumference of the shaft. The blades on the impellers are evenly spaced, and are 0.38 mm tall (the slots are 0.38 mm tall). The backward curved 4-blade impeller has β_1 and β_2 angles of 80 and 85 degrees respectively. The forward curved 4-blade impeller has β_1 and β_2 angles of 146 and 114 degrees respectively.

The top housing is made from acrylic to allow the flow passing into and through the pump to be visualized. The top housing has an inlet channel and outlet channel as seen in Fig. 4, and also has two pressure ports. The first pressure port is connected to the inlet channel passage, as seen in Fig. 4, and is just above the upper bearing at the inlet to the top of the rotary shaft pump. The second pressure port is connected to part of the volute, and comes through the upper bearing into the volute region about two millimeters from the outer surface of the shaft. The diameter of the pressure ports at the fluid channel interface is about 0.4 mm. Each of these then expands to 3.1 mm. The ends of clear plastic tubes are press fit into the 3.1 mm diameter holes, and the opposite ends of the tubes are connected to opposite sides of the pressure transducer. Thus, the pressure transducer measures the differential pressure between the two pressure ports. The bottom housing is made from aluminum, and contains the lower bearing. The bottom housing also has a recess that forms the exit plenum. The

expansion of the fluid channel as it enters the exit plenum slows the fluid, and minimizes losses as the fluid turns to the outlet channel. The bearings are made from Torlon, a strong self-lubricating plastic. The upper and lower bearings are press fit into the top and bottom housing respectively. Torlon is used because it has a low coefficient of friction, and can be easily machined. The outer diameter of the bearings is 6.35 mm, and the inner diameter is 2.38 mm. The locations of these bearings are shown in Fig. 4.

The volute is machined from brass shim stock using a CNC milling machine, and is positioned and designed as seen in Figs. 4 and 5. Each piece of brass shim stock is 104 μm thick. Thus the height of the volute can be changed by stacking pieces of brass shim stock. For all of the present tests, a height of 0.416 mm is used because it is just larger than the height of the slots located in the shaft.

EXPERIMENTAL APPARATUS AND PROCEDURES

The rotary shaft pump is powered by an externally mounted Maxon EC32 number 118891, brushless DC motor that is 32 mm in diameter. The brushless motor is controlled by an Advanced Motion Controls power amplifier (Model #BE12A6). The power amplifier has a DC supply voltage of 40V, a peak current of 12 Amps. A negative feedback controller is employed to maintain constant speed for any variation in torque. The speed is controlled by adjusting a 15-turn potentiometer. The speed range is 100-13,200 rpm. The motor controller determines the rotational speed from the signal from an optical encoder attached to the motor shaft. This apparatus produces a voltage signal that is proportional to speed. The voltage is measured using a Keithley 131 Digital Multimeter.

The test setup is shown in Figure 6 and includes a water reservoir, which is large enough that the water level change during operation is negligible. The outlet channel is connected to the outlet tubing. All outlet tubing is a constant length of 89 mm. The inside diameter of the outlet tubing are changed to throttle the outflow of the rotary shaft pump. The outlet tubing inside diameters (D) are 0.254 mm, 0.508 mm, and 1.397 mm. The pump housing is mounted to the base of a linear slide. The brushless motor and coupling shaft are mounted to the shuttle of the linear slide. The coupling shaft is used to connect the impeller shaft with the motor shaft. The coupling shaft is made from aluminum, and is secured by ball bearings at each end. The rotary shaft pump impeller shaft is connected to the coupling shaft. The position of the shuttle, along with the motor and impeller shaft, are adjusted and secured using 4-40 positioning bolts. There is one positioning bolt at each of the two ends of the shuttle, such that one positioning bolt is used to adjust the position, and the other is used to immobilize the shuttle. A microscope is used to aid the positioning of the impeller shaft by means of the positioning bolts. The microscope is an Infinevar Continually-Focusable Microscope (CFM) (0-330X magnification), manufactured by Infinity Photo-Optical Co., with a Hitachi HV-C20U-S4 video camera connected to a Sony Tinitron PVM-14N5U high resolution monitor.

The pressure ports in the pump housing, shown in Fig. 4, are connected to a DP-15 differential Validyne pressure sensor through two tubes. The pressure sensor diaphragm used in this transducer has a full range of 0-3.5 kPa. The range of pressure

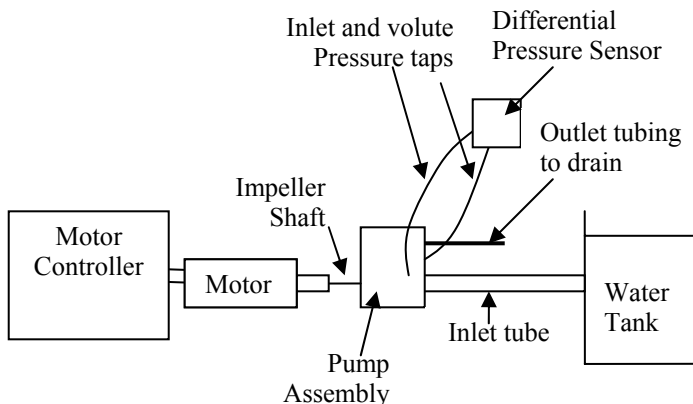


Figure 6. Experimental testing apparatus. Differential pressure sensor measures pressure rise across the pump. Motor controller has an output signal for shaft speed and motor current

measurements during testing is 0-2.1 kPa. The output signal from the pressure sensor is processed using a Celesco Model number CD10D Carrier Demodulator, which produces a voltage output that is proportional to pressure. The voltage is measured by a Keithley 131 Digital Multimeter.

A type-T thermocouple made by Omega Engineering Inc. (Part # TT-T-36-SLE) is used in several experiments to determine the temperature rise through the impeller. Figure 4 shows that the thermocouple is positioned next to the side wall of the volute, about 2 mm from the outer surface of the shaft. The signal from the thermocouple is measured by an HP 3497A data acquisition control unit that electronically compensates for a reference voltage level at 0 degrees Celsius. Temperature measurements indicate that the water temperature increases 1-2 degrees Celsius while traveling through the impeller for rotational speeds of 1000-13,200 rpm. Due to the small range in temperature rise, constant fluid properties is a good assumption for the water employed as the working fluid.

Pump assembly starts by connecting the impeller shaft to the coupling shaft on the motor. The bottom housing is then mounted to a plate on the face of the linear slider, and the position of the slots is adjusted so that the bottom of the slots is flush with the top surface of the bottom housing. The volute is then positioned and secured in place. The top housing is then secured, and tightened to minimize leakage. The inlet and outlet tubes are then connected to the top housing. After assembly and positioning of the impeller shaft and housing, all the air is bled from the system using a syringe attached to the end of the inlet tubing. This includes the inlet channel, outlet channel, and tubing to and from the pressure sensors. After these steps are completed, testing is comprised of the following procedures. (1) The system is flushed to ensure there are no air bubbles or trapped particulates in the pumping chamber. (2) The pump motor is activated, and adjusted to produce the desired speed. (3) The pump then continues to operate at constant speed until steady state is reached, which usually requires 20-30 seconds. (4) The timer is started, and water from the outlet tubing is collected. Output signals related to shaft rotational speed, pressure rise, and volumetric flow rate are then collected. The flow rate is determined by dividing the amount of water collected by the collection time. All data are

Table 1. Uncertainties Associated with Experimental Data

Variable	Percent Uncertainty at 2,640 rpm	Percent Uncertainty at 7,920 rpm	Percent Uncertainty at 13,200 rpm
H_{th}	5%	2.5%	2%
H_{act}	15%	3%	1%
H_{σ}	15%	3%	2%
Q	5%	4%	3%
Rotational speed (rpm)	1%	<1%	<1%

recorded, and then entered and processed using a Microsoft Excel XP software.

EXPERIMENTAL UNCERTAINTY ANALYSIS

A first order uncertainty analysis is performed using Constant-Odds Combination method, based on a 95% confidence level as described by Moffat [18]. Table 1 present uncertainties associated with experimental data. The uncertainty is greatest at low rotational speed, and pressures, due to the small signal to uncertainty ratios. The uncertainty decreases significantly as the rotational speed and pressure increase.

RESULTS AND DISCUSSION

The experimental results are presented in two sections. The first section discusses pressure and flow rate variations for the radial 2-blade, radial 4-blade, radial 6-blade, backward-curved 4-blade, and forward-curved 4-blade impeller configurations for a constant rotational speed. The second section discusses the performance characteristics of the radial 6-blade impeller and the backward curved 4-blade impeller over a range of rotational speeds. Each impeller design is tested using outlet tubing diameters of 0.254 mm, 0.508 mm, and 1.397 mm of the same length.

Trends for Different Impeller Designs

The variations of pressure head with volumetric flow rate for macro-scale pumps with different impeller blade configurations are shown in Fig. 2. Figure 7 shows these same quantities for different RSP impeller designs, all for an impeller rotational speed of 9,240 rpm. To obtain the data presented in Fig. 7, the flow is throttled in the rotary shaft pump experiments by changing the inside diameter of the outlet tubing. All outlet tubing is a constant length of 89 mm. The flow circuit determines the head requirements for a given flow rate through the tubing and pump, and can be determined using the Darcy friction factor and minor loss correlations for expansions and contractions [15]. By decreasing the outlet tubing diameter, with constant length, the flow resistance out of the pump is changed, which changes the pressure rise and flow rate for a constant rotational speed. This arrangement is thus used to provide information on the performance of the rotary shaft pump over a range of rotational speeds, flow rates, and pressure rises.

The data in Fig. 7 for each pump arrangement (from left to right) correspond to outlet tubing inner diameters (D) of 0.254 mm, 0.508 mm, and 1.397 mm, respectively. For each impeller

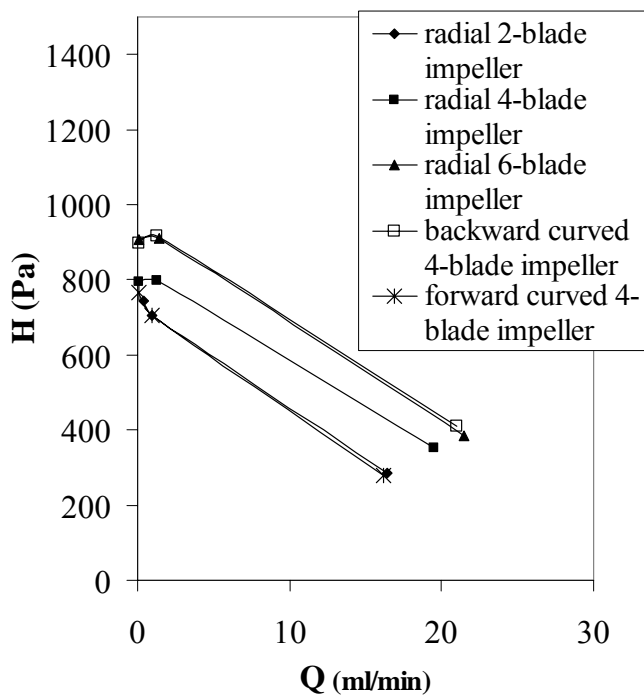


Figure 7. Variation of pumping head with volumetric flow rate data for different impeller designs, where each data set is obtained at a constant impeller rotational rate of 9,240 rpm. The data points, from left to right for each impeller configuration, are obtained with outlet tubing diameter of 0.254 mm, 0.508mm, and 1.397 mm, respectively.

configuration (operating at constant impeller rotational speed), Fig. 7 shows that increasing the exit tube diameter gives a higher volumetric flow rate through the pump, which, for the impellers tested, gives lower magnitudes of pressure head. The pumping head measured at intermediate flow rates (5-15 ml/min) for the forward curved and backward curved 4-blade impellers are obtained for a rotational speed of 9,240 rpm, with an outlet tubing inner diameter of 1.397 mm, with length of 195 mm and 603 mm. The pumping head measured with these conditions are consistent with the data lines in Fig. 7. Qualitative trends of Fig. 7 data for each impeller configuration (at constant impeller rotational speed) are similar for $Q > 2$ ml/minute. Here, different data sets have similar slopes, sometimes with different ranges of pump head. At lower volumetric flow rates, data sets for different impeller configurations sometimes show completely different slopes, as well as different quantitative trends. Overall, data trends shown in Fig. 7 are similar to ones also observed at impeller rotational speeds of 1,320 rpm and 13,200 rpm. Pressure head magnitudes produced by the impeller generally decrease as the flow rate is increased (as outlet tubing diameter increases) for a constant rotational speed. This is associated with a decrease of hydraulic efficiency, which is related to overall impeller behavior, and to increased hydrodynamic losses and increased slip as flow rate increases. The nearly parallel nature of the pressure rise and flow rate trends for the different impeller blade designs indicates that these overall slopes are independent of impeller blade design. The impeller blade design thus appears to affect

the magnitude of the product of hydraulic efficiency and slip factor, but not overall slopes of the pressure - flow rate data. Average values of the hydraulic efficiency and slip factor product over the range of impeller rotational speeds from 1320 to 13,200 rpm, for each individual impeller blade design, are presented in Table 2.

Table 2. Average values of $\eta\sigma$ for rotational speeds from 1,320 rpm to 13,200 rpm for various impeller designs

Impeller Configuration	Average value of $\eta\sigma$		
	$D=0.254$ mm	$D=0.508$ mm	$D=1.397$ mm
Radial 2-blade impeller	0.58	0.565	0.278
Radial 4-blade impeller	0.621	0.581	0.339
Radial 6-blade impeller	0.683	0.687	0.346
Backward curved 4-blade impeller	0.706	0.714	0.343
Forward curved 4-blade impeller	0.586	0.576	0.261

Performance Characteristics of the Pumps with the Backward-Curved 4-Blade Impeller and the Radial 6-Blade Impeller

Figures 8a and 8b show the variation of pressure change with flow rate for the radial 6-blade impeller and for the backward curved 4-blade impeller, respectively, obtained with outlet tubes of different inner diameters. Each data point is taken at steady state with a constant impeller rotational speed ranging from 1,320 to 13,200 rpm. As the rotational speed is increased, the pressure rise and flow rate also increase for each configuration. As seen from Table 2, the product of hydraulic efficiency and slip factor changes with different pump configurations. The configuration with the 1.397 mm outlet tubing has the highest flow rates, but also has the lowest product of hydraulic efficiency and slip factor. This is tied to impeller performance at higher flow rates. Note that greater viscous stresses are also present at higher flow rates in the larger diameter tubes because of larger velocity gradients.

The different outlet tubing diameters change the characteristics of the fluid circuit. Each different fluid circuit, each with a different outlet tubing diameter, is represented on Fig. 8 by a line starting at the origin which emanates through the data points which extend from the origin. These theoretical lines in Fig. 8 are determined by setting the pumping head from Eq. (1) equal to the major and minor pressure losses through the fluid circuit associated with laminar flow through a pipe or channel with expansions and bends [16], which results in a linear relationship between flow rate and pumping head. The slope of each line is mostly determined by the outlet tubing diameter, inlet tubing, other parts of the fluid channel, as well as impeller performance. The position of the data along the line is governed by pump impeller configuration, rotational speed, hydraulic efficiency, and slip factor. The data given in Fig. 8 are given for the backward curved 4-blade impeller and the radial 6-blade impeller because these produce the highest

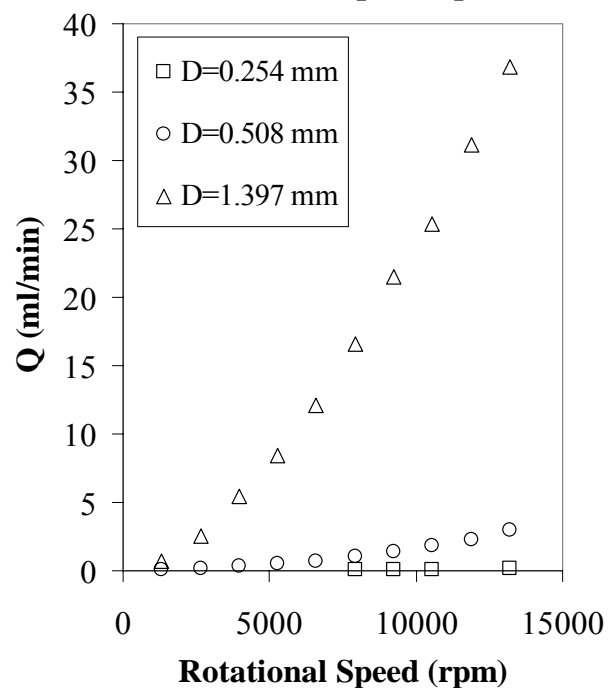
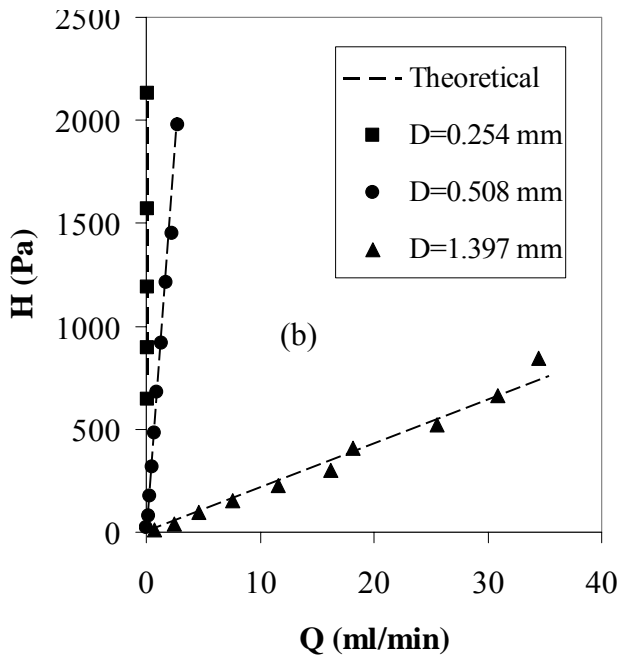
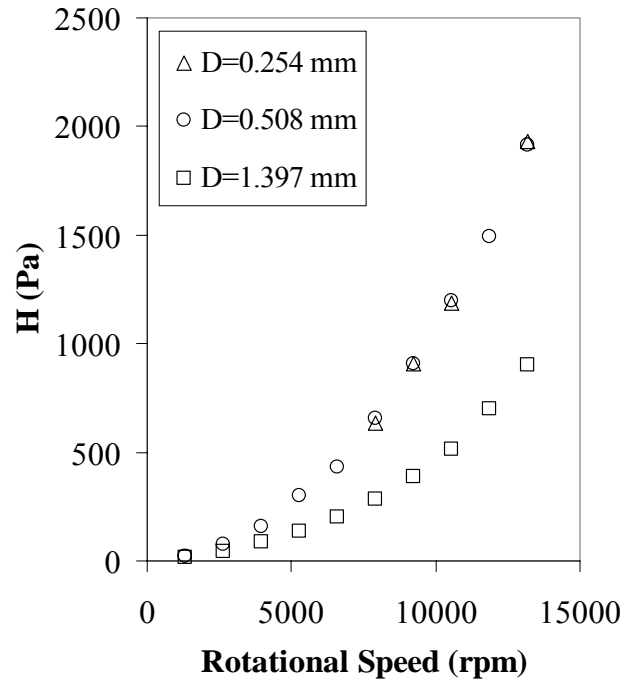
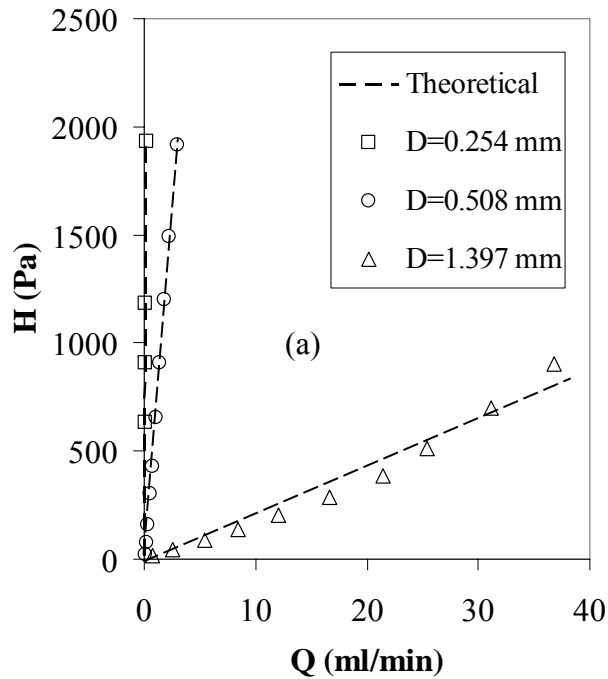


Figure 8. Pressure rise and flow rate data for the (a) radial 6-blade impeller and the (b) backward curved 4-blade impeller. Data are taken with impeller rotational speeds from 1320 rpm to 13,200 rpm.

Figure 9. Pressure rise and flow rate data for different rotational speeds for the radial 6-blade impeller. Data are taken with impeller rotational speeds from 1320 rpm to 13,200 rpm.

pressure rise at a particular flow rate, and also have the highest efficiency and slip factor. Of the pumps tested, this indicates that the best millimeter-scale pump has backward curved blades, and 4-6 impeller blades.

Figures 9 and 10 show pressure change and flow rate as they depend on rotational speed of the impeller for the radial 6-blade impeller and for the backward curved 4-blade impeller, respectively. Each data point is taken at the same experimental conditions as the data given in Figs. 8a and 8b. Figure 11 shows the pressure change and rotational speed squared for the backward curved 4-blade impeller and the radial 6-blade

impeller. The data in Fig. 11 indicates a nearly linear relationship between pumping head and rotational speed squared (outer blade tip velocity squared) as suggested from eq. (1). From the data presented, it is apparent that the flow rate can be changed easily by adjusting the rotational speed of the impeller and by changing outlet tubing diameter and length. The minimum and maximum flow rates shown in Fig. 8 are 0.06 ml/min, and 34.5 ml/min, respectively. The maximum flow rate obtained for both impeller configurations is about

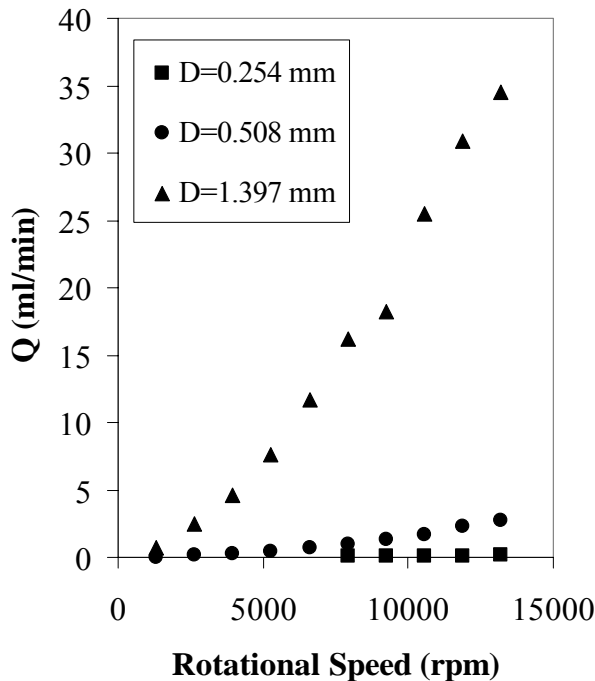
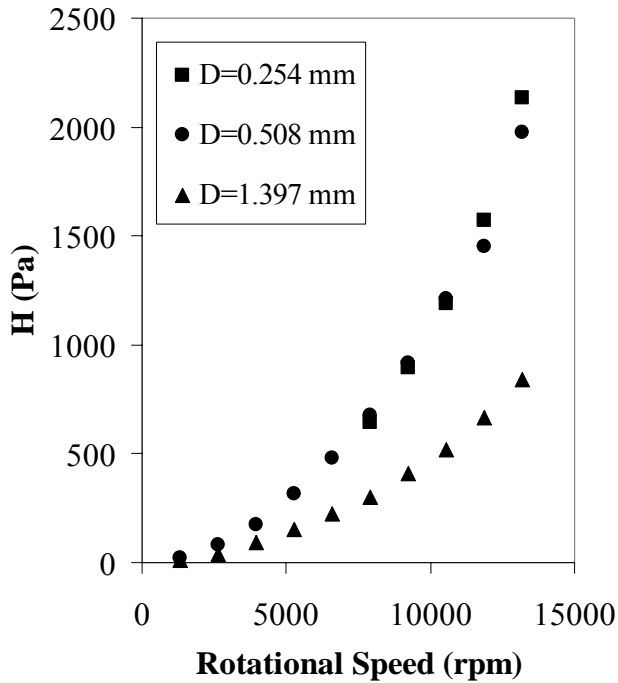


Figure 10. Pressure rise and flow rate data for different rotational speeds for the backward curved 4-blade impeller. Data are taken with impeller rotational speeds from 1320 rpm to 13,200 rpm.

64.9 ml/min at a rotational speed of 13,200 rpm, with an outlet tubing diameter of 4.5 mm. Note that greater pressure rises and greater flow rates are present at higher rotational speeds. The maximum pressure obtained at a rotational speed of 13,200 rpm is about 2.1 kPa for both impeller configurations.

Figure 12 shows a plot of the product of hydraulic efficiency and slip factor for different rotational speeds for the radial 6-blade impeller and the backward curved 4-blade impeller. In Fig. 12, the overall trend of the product of

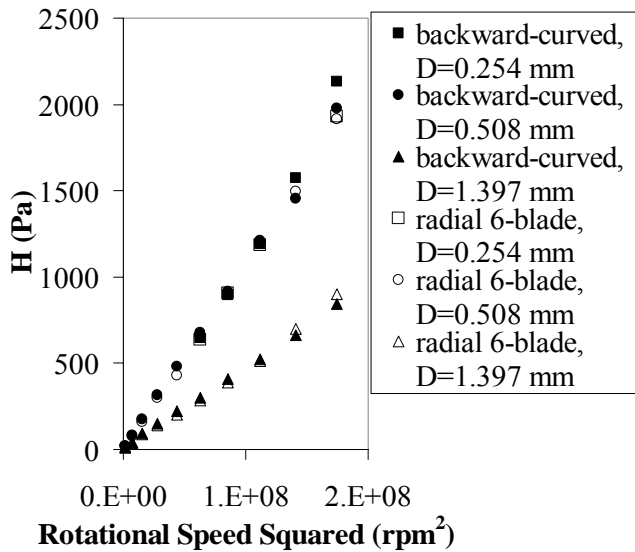


Figure 11. Pressure rise and rotational speed squared for the backward curved 4-blade impeller and the radial 6-blade impeller. Data are taken with impeller rotational speeds from 1320 rpm to 13, 200 rpm.

hydraulic efficiency and slip factor, for an outlet tubing diameter of 1.397 mm, decreases as impeller rotational speed increases. The overall trend of the product of hydraulic efficiency and slip factor, for outlet tubing diameters of 0.254 and 0.508 mm, is a slight decrease as impeller rotational speed increases from 1,320 rpm to 7,920 rpm, and sometimes a slight increase near an impeller rotational speed of 13,200 rpm. The maximum value of this quantity of 0.78 is obtained at high rotational speeds and small flow rates, with the 0.254 mm ID outlet tubing with the backward curved 4-blade impeller. The hollow interior of the centrifugal rotary shaft pump transfers momentum from the shaft to the fluid by viscous forces. The “pre-swirl” due to this momentum transfer means that less acceleration of fluid is needed and provided by the blades, which therefore diminishes the amount of slip. The product of efficiency and slip factor, for the radial 6-blade impeller with the 1.397 mm inner diameter outlet tubing, decreases from 0.55 to 0.35 as the flow rate and rotational speed increases, which implies that the product of efficiency and slip factor continues to decrease for higher impeller rotational speeds and flow rates. The other impeller designs also have decreasing product of hydraulic efficiency and slip factor as the rotation speed increases for an outlet tubing inner diameter of 1.397 mm. For a constant rotational speed of 9,240 rpm, the magnitude of the $\eta\sigma$ product decreases by 58% for the 6-blade radial impeller as the flow rate increases. There is also a difference of 30% in the magnitude of $\eta\sigma$ between the backward curved 4-blade impeller and the radial 2-blade impeller for a constant rotational speed of 9,240 rpm, with the same outlet tubing. This implies that both the impeller design and the flow rate are significant, but the flow rate has a more significant effect on the performance of the rotary shaft pump.

The product of hydraulic efficiency and slip factor for all impeller blade configurations with an outlet tubing inner diameter of 0.508 mm is shown in Fig. 13. The data in Fig. 13 shows that the product of hydraulic efficiency and slip factor can be significantly changed with impeller configuration. The

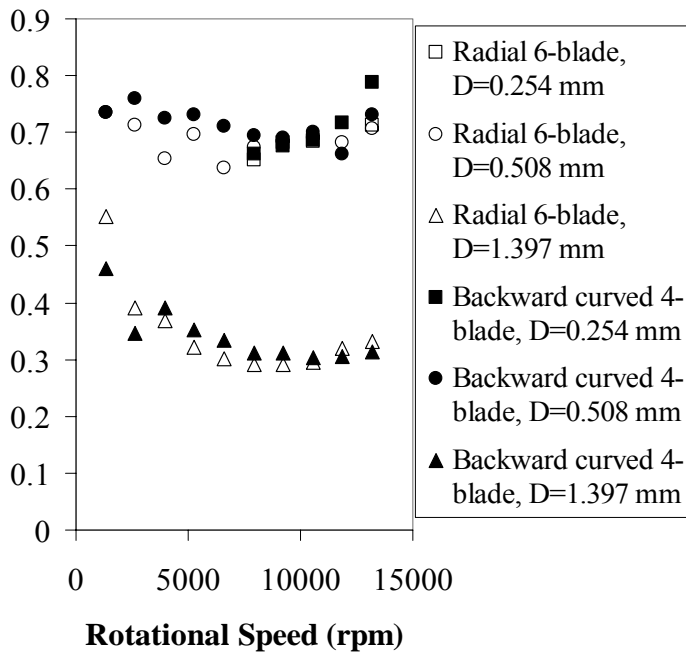


Figure 12. Product of hydraulic efficiency and slip factor for the radial 6-blade impeller and backward curved 4-blade impeller. Data are taken with impeller rotational speeds from 1320 rpm to 13,200 rpm.

most efficient impeller configurations are the radial 6-blade impeller and the backward-curved 4-blade impeller. The impeller configurations with the lowest efficiency-slip factor product are the radial 2-blade impeller and the forward-curved 4-blade impeller.

SUMMARY AND CONCLUSIONS

A novel millimeter-scale rotary micropump called the rotary shaft pump (RSP) is developed, characterized, and tested. The top and bottom of the impeller blades of this device are integral parts of the rotary shaft, which serves as the inlet duct passage to the impeller. This arrangement increases reliability with well supported impeller blades, and reduces risk of blade damage due to contacting the top pump housing. The device is mechanically robust and easy to manufacture. The hollow interior of the RSP transfers momentum to the passing fluid, which is significant on the millimeter-scale employed, and aids the pumping process by inducing circumferential momentum at the inlets of the impeller blades.

The highest hydraulic efficiency-slip factor product of 0.78 is produced by the backward-curved 4-blade impeller with a rotational speed of 13,200 rpm and an outlet tubing inner diameter of 0.254 mm. The presented millimeter-scale RSP produces flow rates up to 64.9 ml/min. This value is larger than many other micropumps [1-4, 6-10], which generally reach flow rates only up to about 16 ml/min. Larger-scale versions of the rotary shaft pump may be ideal for applications in blood pumping, and ventricle assist devices [11-13], chemical analysis systems, drug delivery, and electronics cooling. Smaller-scale versions are ideally suited for chemical analysis systems, μ -TAS, and drug delivery.

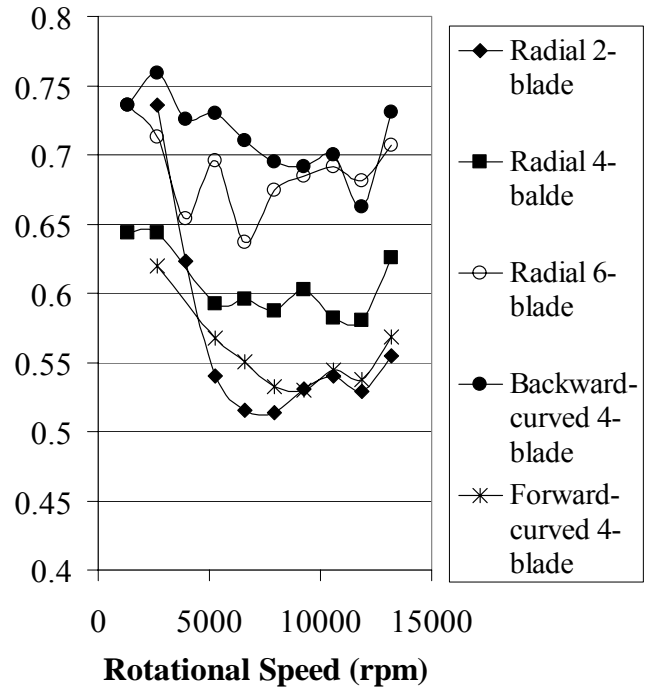


Figure 13. Product of hydraulic efficiency and slip factor for all impeller configurations with an outlet tubing inner diameter (D) of 0.508 mm.

ACKNOWLEDGMENTS

Work presented in this paper was supported by the National Science Foundation (NSF) through the IGERT Program, grant number DGE 9987616.

REFERENCES

- [1] Nhuyen, N-T, Wereley, S. T., 2002, *Fundamentals and Applications of Microfluidics*, Artech House, Inc., Norwood, pp. 292-337.
- [2] Olsson, A., Steeme, G., and Steeme, E., 1995, "A Valve-Less Planar Fluid Pump With Two Pump Chambers," *Sensors and Actuators A: Physical*, **47** (2), pp. 549-556.
- [3] Richter, A. and Sandmaier, H., 2001, "An Electrohydrodynamic Micropump," *Journal of Micro Electro Mechanical Systems*, **10**, (1), pp 98-106.
- [4] Zeng, S., Chen, C. H., Mikkelsen Jr. J. C., and Santiago, J. G., 2000, "Fabrication and Characterization of Electrokinetic Micro Pumps," *7th Intersociety Conference on Thermal and Thermomechanical Phenomena in Electronic Systems*, CPMT/IEEE, Las Vegas, **2**, pp. 31-36.
- [5] Hainan, C., Ahaoying, Z., Yong, L., Xiongying, Y., and Yihua, Y., 1997, "A novel centrifugal miniature pump and its medical application," *Proceedings of the 1997 International Symposium On Micromechatronics and Human Science*, IEEE, pp. 115-117.

- [6] Kilani, M., Galambos, P., Haik, Y., and Chen, C. J., 2003, "Design and Analysis of a Surface Micromachined Spiral-Channel Viscous Pump," *ASME Journal of Fluids Engineering*, **125** (2), pp. 339-344.
- [7] Sen, M., Wajerski, D., and Gad-El-Hak, M., 1996, "A Novel Pump for MEMS Applications," *ASME Journal of Fluids Engineering*, **118**, (3), pp. 624-627.
- [8] Ahn C. H. and Allen, M. G., 1995, "Fluid micropumps based on rotary magnetic actuators," *Proceedings of IEEE Micro Electro Mechanical Systems 1995*, IEEE, ASME, pp. 408-418.
- [9] Cao, L., Mantell, S., and Polla, D., 2000, "Implantable medical drug delivery system using microelectromechanical system technology," *First Annual International Conference of Microtechnologies in Medicine and Biology*, pp. 487-490.
- [10] Tas, N. R., Berenschot, J. W., Sanders, R. G. P., Lammerink, T. S. J., Elwenspoek, M., and Van der Berg, A., 2001, "Bubble pump for integrated nanofluidics," *Proceedings of 2001 First IEEE Conference of Nonotechnology*, IEEE, Maui, pp. 454-458.
- [11] Shen, J.X., Tseng, K.J., Vilathgamuwa, D.M., and Chan, W.K., 2000, "A Novel Compact PMSM with Magnetic Bearing for Artificial Heart Application," *IEEE Transactions On Industry Applications*, **36**, (4), pp. 1061-1068.
- [12] Wan, S. and Tseng, K.J., 2001, "Novel Bearingless Centrifugal Blood Pump," *Proceedings of the Fourth International Conference on Power Electronics and Drive Systems*, Istitute of Electrical and Electronics Engineers Inc. Denpasar, **2**, pp. 743-748.
- [13] Nishimura, K., Park, C-H., Akamatsu, T., Yamada, T., and Ban, T., 1996, "Development of a magnetically suspended centrifugal pump as a cardiac assist device for long-term application," *American Society for Artificial Internal Organs (ASAIO) Journal*, **42**, (1), pp. 68-71.
- [14] Karniadakis, G.E., Beskok, A., 2002, *Micro Flows, Fundamentals and Simulation*, Springer, New York, pp. 1-31.
- [15] Blanchard, D., Ligrani, P., Gale, B. "Centrifugal Micropump," Provisional Patent: University of Utah Attorney Docket Number U2550P.1.
- [16] Fox, and McDonald, 1998, *Introduction to Fluid Mechanics, Fifth Edition*, John Wiley & Sons, Inc., New York, pp. 493-522.
- [17] Gorla R.S.R. and Khan, A.A., 2003, *Turbomachinery, Design and Theory*, Marcel Dekker, Inc., New York, pp. 47-90.
- [18] Moffat, R.J, 1982, "Contributions to the Theory of Single-Sample Uncertainty Analysis," *Journal of Fluids Engineering*, **104**, pp. 250-260.